

Evolution and scaling of a simulated downburst-producing thunderstorm outflow

Christopher Oreskovic^{1a}, Eric Savory^{*1}, Juliette Porto^{2b} and Leigh G. Orf^{3c}

¹Department of Mechanical and Materials Engineering, University of Western Ontario, Canada

²Ecole Nationale Supérieure de l'Energie, Eau et Environnement (ENSE3)
Institut Polytechnique de Grenoble, France

³Cooperative Institute for Meteorological Satellite Studies, University of Wisconsin-Madison Wisconsin, USA

(Received October 12, 2017, Revised December 27, 2017, Accepted January 15, 2018)

Abstract. For wind engineering applications downbursts are, presently, almost exclusively modeled, both experimentally and numerically, as transient impinging momentum jets (IJ), even though that model contains none of the physics of real events. As a result, there is no connection between the IJ-simulated downburst wind fields and the conditions of formation of the event. The cooling source (CS) model offers a significant improvement since it incorporates the negative buoyancy forcing and baroclinic vorticity generation that occurs in nature. The present work aims at using large-scale numerical simulation of downburst-producing thunderstorms to develop a simpler model that replicates some of the key physics whilst maintaining the relative simplicity of the IJ model. Using an example of such a simulated event it is found that the non-linear scaling of the velocity field, based on the peak potential temperature (and, hence, density) perturbation forcing immediately beneath the storm cloud, produces results for the radial location of the peak radial outflow wind speeds near the ground, the magnitude of that peak and the time at which the peak occurs that match well (typically within 5%) of those produced from a simple axi-symmetric constant-density dense source simulation. The evolution of the downdraft column within the simulated thunderstorm is significantly more complex than in any axi-symmetric model, with a sequence of downdraft winds that strengthen then weaken within a much longer period (>17 minutes) of consistently downwards winds over almost all heights up to at least 2,500 m.

Keywords: downburst; CM1 cloud model; thunderstorm; numerical modeling

1. Introduction

Downbursts are masses of air that descend rapidly from thunderstorms in the lower atmosphere and impact the ground, resulting in large radial outflows of intense winds that have the potential to damage buildings and other structures (Shehata *et al.* 2005, Abd-Elaal *et al.* 2013, Aboshosha and El Damatty 2015). Downbursts are density driven events, resulting from the thermodynamic cooling of the earth's atmosphere associated with processes occurring within thunderstorm clouds. Thermodynamic processes, evaporation of rain and the melting/sublimation of snow and graupel create pockets of negatively buoyant air which, eventually, descend towards the ground. Due to the downburst's strong time dependence and spatial variation, field measurements can be particularly challenging, but have become more extensive in recent years (Holmes *et al.* 2008, Lombardo *et al.* 2014, Solari *et al.* 2015, Gunter and

Schroeder 2015, Burlando *et al.* 2017, Zhang *et al.* 2017). Although such field data have yielded vertical profiles of downburst radial wind speeds, residual turbulence (by applying moving averaging) and gust factors, they do not reveal any quantitative connection between those metrics and the physics of the parent storm. Currently, in wind engineering research, physical studies and numerical simulations of the downburst phenomenon have been mostly limited to the axi-symmetric, impulsively-driven impinging circular jet, better known as the IJ model (Sengupta *et al.* 2001, Letchford and Chay 2002, Kim and Hangan 2007, Sengupta and Sarkar 2008). Further, in meteorological research the principal method of studying downbursts is the cooling source (CS) model (Anderson *et al.* 1992, Orf and Anderson 1999, Mason *et al.* 2009, Vermeire *et al.* 2011a,b, Zhang *et al.* 2013), which is created by specifying an axi-symmetric cooling forcing function that represents the dominant thermodynamic cooling present in natural thunderstorm formation. However, these two traditional downburst models have tangible limitations as both ignore the realistic physical effects that occur in the natural formation of a downburst event, such as the microphysical thermodynamic processes that lead to the formation of the event itself, as well as other phenomena such as drag-induced downflow due to the presence of falling hydrometeors (Mason *et al.* 2009, Anabor *et al.* 2011). In addition to this, the IJ model utilizes the unrealistic forcing of an impulsively started jet which does not occur in nature (Zhang *et al.* 2013).

*Corresponding author, Professor

E-mail: esavory@uwo.ca

^a MSc Student

E-mail: coresko2@uwo.ca

^b MSc Student

E-mail: Juliette.Porto@ense3.grenoble-inp.fr

^c Research Scientist

E-mail: leigh.orf@ssec.wisc.edu

What remains unclear is whether a distinct relationship exists between the physical size and density perturbation of a downburst “source” region within a thunderstorm and the intensity of the downburst outflow velocities, particularly those near the ground. The overall goal of the present research is to determine if scaling parameters exist for realistic thunderstorm numerical models, similar to that previously developed for the IJ model. That model linearly relates the peak velocity and the diameter of the impinging jet momentum source to the peak outflow velocity and the location at which that peak occurs, respectively (Kim and Hangan 2007, Shehata *et al.* 2005). The present authors have developed a unique, very high-resolution simulation methodology (Orf *et al.* 2012) which utilizes the CM1 cloud model (Bryan and Fritsch 2002). This is a sophisticated, physically-realistic, large-scale downburst-producing thunderstorm large-eddy simulation (LES) numerical model, which includes realistic microphysical formulations. More recently, a temporal analysis of the evolution of a CM1 Cloud Model simulated downburst event has been conducted (Orf *et al.* 2014), expanding on previous circumferential analysis of the same numerical model. Building upon that prior work the present paper seeks to answer the following questions:

- (1) To what extent does a modelled thunderstorm produce a distinct downburst event that resembles those produced by simpler physical and numerical downburst models?
- (2) Can the downburst produced by a thunderstorm be scaled using a simple approach, based on a density perturbation at the “source” of the downburst within the cloud?

In order to answer these questions the temporal and spatial wind distributions associated with the downburst as it evolves are examined and the circumferentially-averaged wind speed data are tested against the simplest model available for density-driven downburst events, namely the downburst scaling developed by Lundgren *et al.* (1992) based on laboratory scale experiments involving dense liquid releases. Here, the results from using that model are supplemented by data from Unsteady Reynolds-Averaged Navier-Stokes (URANS) numerical simulations of similar liquid releases. The next section briefly describes the CM1 cloud model, followed by the URANS simulation methodology, including the grid independence and validation studies. Then, the scaling method is introduced, followed by the results from the simulations and their discussion.

2. Numerical modelling details

The following sub-section summarizes the cloud model (full details are available in Bryan and Fritsch 2002), with specific details relating to the present application being given in Orf *et al.* (2012). The subsequent section covers the two-fluid URANS simulations of dense liquid releases.

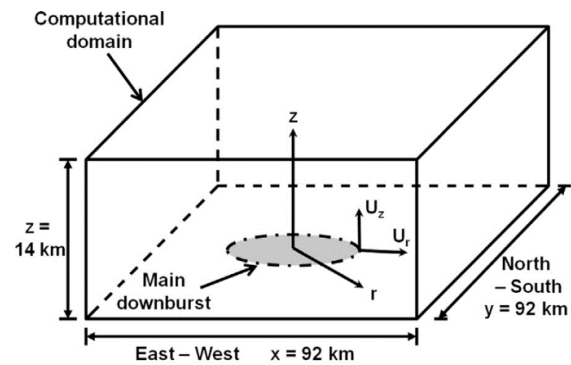


Fig. 1 Sketch of the thunderstorm model domain showing dimensions and co-ordinate systems

2.1 Full thunderstorm cloud model (LES model)

The numerical model used to capture the realistic physics of the formation and evolution of a downburst-producing thunderstorm is the CM1 Bryan cloud meteorological model Version 13 (Bryan and Fritsch 2002). CM1 is a fully three-dimensional atmospheric model that makes use of finite differencing methods to solve for three components of wind velocity, potential temperature perturbation, non-dimensional pressure and other microphysical variables. This model is non-hydrostatic, taking into account vertical accelerations typically present in realistic thunderstorm conditions. A semi-slip boundary condition is used in this work, with a ground roughness (z_0) of 0.1 m, as utilized in earlier CS and IJ models (Vermeire *et al.* 2011a,b). The model domain has the highest resolution grid spacing in both the vertical and horizontal directions at positions near the ground focusing on the area of the storm where the downburst occurs. The domain consists of a three-dimensional volume of $92 \times 92 \times 14 \text{ km}$ with constant horizontal grid spacing of 20 m in the centre of the domain. A vertical grid spacing of 5 m is present from $z = 2.5 \text{ m}$, increasing to 95 m at the top of the domain ($z = 14 \text{ km}$). Fig. 1 illustrates the dimensions of the computational domain and defines the principal geometrical and wind speed parameters.

The model was initialized using a horizontally homogenous base state derived from the composite atmospheric sounding reported by Brown *et al.* (1982). This vertical profile of temperature, pressure, humidity and horizontal winds (Fig. 2) was constructed from observations of several downburst-producing thunderstorms near Boulder, CO, at the Front Range of the Colorado Rockies. This profile is characteristic of a dry-microburst producing environment often found in the US High Plains, containing weak vertical wind shear and exhibiting a 4.5 km deep, well-mixed neutrally-stable (dry adiabatic) boundary layer beneath a 5 km region of conditional instability that contains the bulk of the cloud. Because the simulation is run in an environment containing vertical wind shear, the resulting cloud and subsequent downdrafts are fully three-dimensional features that do not exhibit axi-symmetry despite the storm being forced with an axi-symmetric “warm bubble” temperature perturbation. This forcing

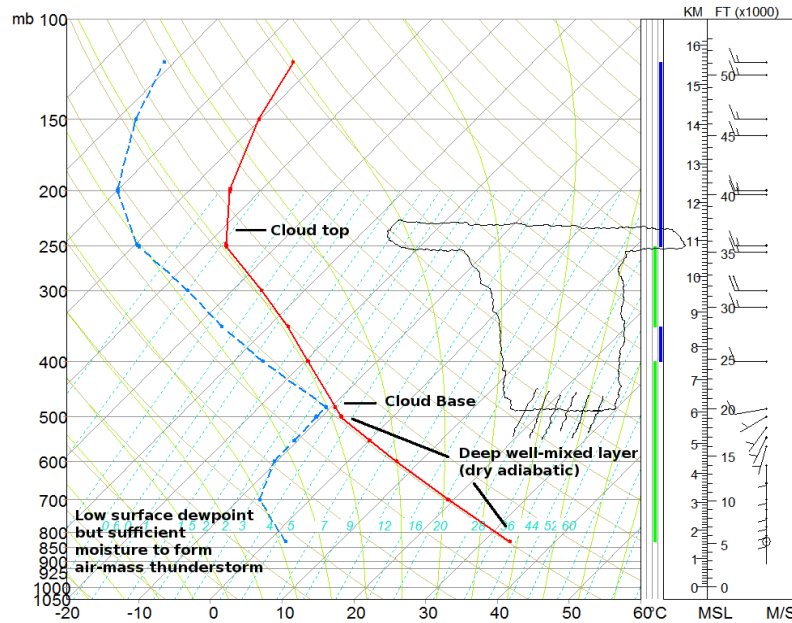


Fig. 2 Skew-T/log-p diagram of the atmospheric conditions that serve as the base state for the CM1 simulation. The solid red line indicates the atmospheric temperature, while the dashed blue line represents the dewpoint temperature, both in degrees Celsius. The cartoon cloud roughly indicates the vertical extent of the simulated thunderstorm, which produces rain and snow that falls (and melts to form rain). Rain in the neutral boundary layer readily evaporates, forming negatively buoyant pools of air that accelerate downward, forming the downburst. The drag of the falling rain also serves to force air downward, but is of secondary importance (adapted from Brown *et al.* 1982)

creates positive buoyancy that results in convection in the lower atmosphere that triggers the thunderstorm. The location of the “warm bubble” was manipulated until a downburst was produced by the modeled thunderstorm in the centre of the model domain, where the mesh is most dense. Surface air parcels lifted in this environment become saturated at approximately 4.5 km above ground level (AGL) which defines the lifted condensation level (LCL), or cloud base height. In this environment, the LCL is also the level of free convection (LFC), and air parcels lifted to this level will convect freely until reaching the tropopause approximately 5 km above the LCL. As is the case with such environments, rain and snow formed within the cloud will descend into the dry-neutral boundary layer where thermodynamic processes (melting, sublimation and evaporation) create pockets of negatively buoyant air that are free to descend, driving the downdrafts that form the downbursts.

2.2 Dense fluid release model (URANS model)

As mentioned in the introduction, the only established experimental model for simulating density-driven downbursts involves the release of a dense liquid parcel into a less dense ambient liquid, first introduced in Lundgren *et al.* (1992) with additional results presented by Yao and Lundgren (1996). They used a saltwater solution for the source and freshwater for the ambient, a combination that was modified (Alahyari 1995, Alahyari and Longmire 1994, 1995) to provide more realistic viscosity differences between the fluids as well as refractive index matching to

allow for reliable laser-based flow field measurements. More recently, one of the present authors has developed this approach to incorporate a mechanical drop release mechanism for the dense fluid cylinder and to allow traversing of the cylinder within an ambient storm translation (Roberto *et al.* 2015). In the present numerical simulations of such liquid releases the modelled fluid release cylinder had an internal diameter of 75 mm and a height of 76 mm, to match the experimental device in Roberto *et al.* (2015), with the 2-D axi-symmetric geometry realized on the ANSYS Workbench, the mesh in ICEM 14.5 and the simulations conducted using Fluent 14.5. The simulations solved the Unsteady Reynolds-Averaged Navier-Stokes (URANS) equations, with the $k-\omega$ turbulence closure incorporating the low-Re correction. The computational domain is illustrated in Fig. 3 that also shows the boundary conditions. The vertical height was chosen to match the vertical depth of the ambient fluid whilst the radial width of 300 mm was selected, after running several trials, to be the minimum domain size that did not influence the flow in the near-wall outflow region. The solutions were found to be independent of time step size for $\Delta t = 0.001$ sec and 50 iterations were required at each time step, with the residuals being under 10^{-6} , except for continuity which was 10^{-4} .

Six computational meshes were examined in order to achieve an optimum grid size. Fig. 4(a) shows the variation with time of the domain wide maximum velocity magnitude, whilst Fig. 4(b) illustrates the vertical profile of the radial wind speed component at the time and radial location corresponding to where its maximum value occurs.

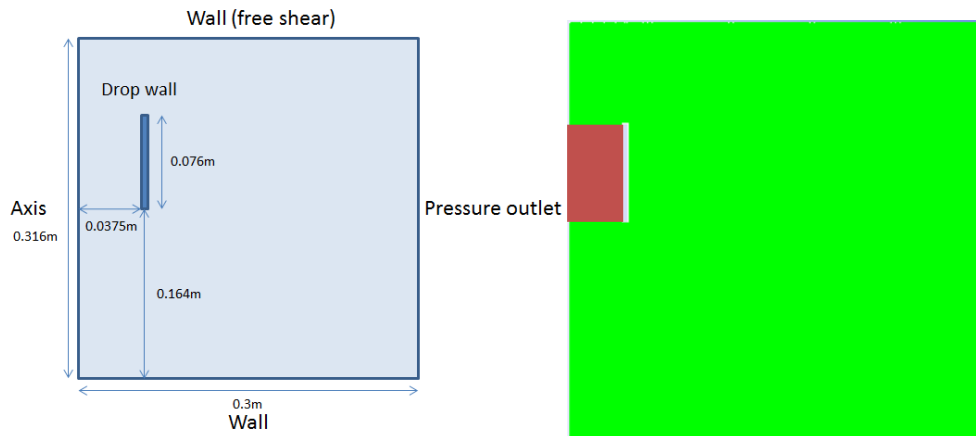


Fig. 3 Axi-symmetric computational domain for URANS simulations of dense fluid releases (left: geometry, right: domain with region containing the dense fluid in red and drop cylinder wall in white)

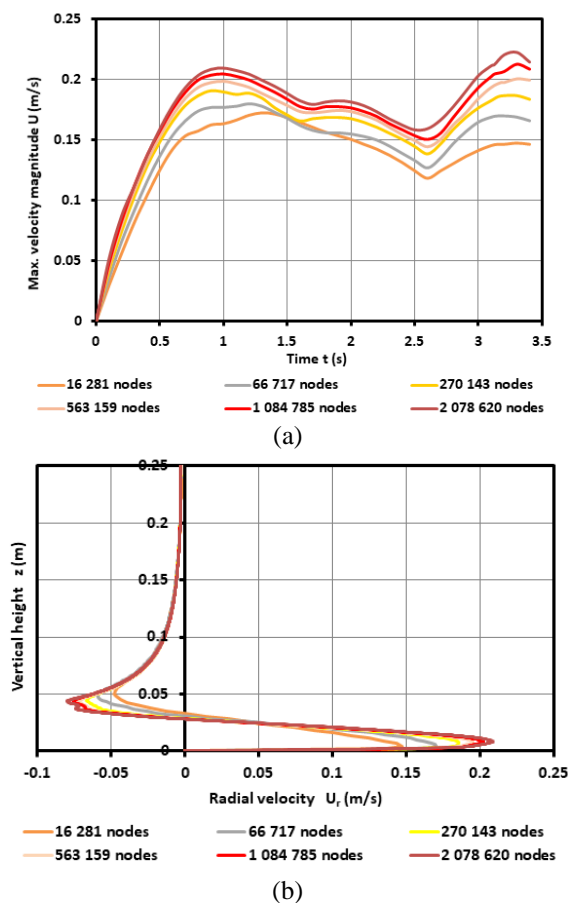


Fig. 4 URANS grid independence study: (a) Variation with time of domain wide maximum velocity magnitude and (b) Vertical profile of the radial velocity at the radial location and time corresponding to the maximum radial velocity

In the case of the radial velocity profile the root mean square deviation over the whole profile between the two finest meshes was 0.04% with the difference in the peak value being 3.08%. It was not considered feasible to achieve grid independence for this peak value by continued refinement and so the second finest mesh of approximately

1 million nodes was selected for all further simulations. For this mesh condition the largest CFL number was 0.65 which is considerably less than the maximum allowable value of 4 for an acceptable simulation. The maximum y^+ value at the wall was 0.45.

Table 1 Density and dynamic viscosity of the simulated fluids

Fluid	Density (kg/m ³)	Dynamic viscosity (kg/ms)
Ambient fluid	1014.40	0.00121
Dense fluid: 3% density difference	1045.77	0.00113
Dense fluid: 4% density difference	1056.67	0.00116

3. Scaling method and validation

As noted previously (Orf *et al.* 2014), the reason why the IJ model continues to be used in wind engineering, even though it models *none* of the physics of real events, is because of its simplicity, notably the linear scaling of both the wind velocity vector with the jet nozzle exit peak velocity and spatial positions with the jet nozzle diameter. Since real events have neither a nozzle nor an initial momentum jet, it is necessary to seek another scaling method if some of the real physics are to be incorporated. Parameters, developed by Lundgren *et al.* (1992), based on the primary forcing mechanism of a density difference between the downburst air and the surrounding ambient air, allow scaling between modelled events and full-scale downbursts. The length scale, R_0 , which is the equivalent spherical radius of the initial volume of relatively dense downburst fluid, is defined as shown in Eq. (1(a)), where Q is the volume of the dense fluid. The corresponding time scale, T_0 , is given in Eq. (1(b)) where ρ is the ambient fluid density and $\Delta\rho$ is the density difference between the downburst and the ambient fluid. A velocity scale, V_0 , is then defined by dividing the length scale by the time scale Eq. (1(c)). Using these scales an expression for the Reynolds number (Re) is obtained Eq. (1(d)), where ν is the kinematic viscosity, which is, for convenience, taken to be that of the ambient fluid.

$$\begin{aligned}
 \text{a) } R_0 &= \left(\frac{3Q}{4\pi}\right)^{1/3} & \text{b) } T_0 &= \left(\frac{R_0\rho}{g\Delta\rho}\right)^{1/2} \\
 \text{c) } V_0 &= R_0/T_0 & \text{d) } Re &= \frac{V_0 R_0}{\nu}
 \end{aligned}
 \quad (1)$$

Note that this model does not include any other downdraft forcing, such as precipitation drag, and nor does it account for any vertical variation in environmental parameters. However, it does contain the primary forcing mechanism of negative buoyancy. It may be seen that the relationship between the source intensity (represented in T_0) and the resulting velocities (as indicated by V_0) is *non-linear*, to the first order at least, unlike the IJ relationship. Lundgren *et al.* (1992) studied two sizes of release cylinder, $R_0 = 26.7$ and 34.0 mm, whilst Alahyari and Longmire (1994, 1995) used $R_0 = 38.8$ and 45.2 mm. The present URANS simulations are for $R_0 = 43.1$ mm with the height of the base of the cylinder above the ground plane being $H_0 = 3.81 R_0$ to match with the above-mentioned previous work. Lundgren *et al.* (1992) established that the large-scale dynamics of the downburst were independent of Re for $Re > 3 \times 10^3$. In the present URANS simulations, the lowest value of Re (for the smallest density difference of $\Delta\rho/\rho = 0.03$) was 4.4×10^3 . The properties of the fluids examined in the numerical modelling are given in Table 1.

Although not shown here, for conciseness (but reported in Roberto *et al.* 2015), the URANS simulations for different density differences confirm that, for a given geometrical arrangement, the velocity fields scaled by V_0 collapse onto single curves when spatial locations are normalized by R_0 and the time during the event is scaled by T_0 . To demonstrate the general validity of the model, Fig. 5(a) shows results for the variation with time of the height (H) of the downburst front, whilst Fig. 5(b) shows the corresponding radius (r_m), in the horizontal direction, of the downburst front, for different studies.

From Fig. 5(a) it can be seen that the dense fluid accelerates after it begins falling, and then impinges on the ground plane at $t/T_0 \approx 6$. The vertical velocity of the initially stationary downburst front reaches a non-dimensional velocity of around 0.25 at $t/T_0 = 1$, increasing to about 0.83 when the downburst is accelerating toward the ground plane at $t/T_0 = 4$. Over the whole descent of the front the two sets of experimental data (Lundgren *et al.* 1992, Roberto *et al.* 2015) and the URANS simulation results all agree to within a root mean square deviation of 5%. The agreement between these studies, in terms of the radial width of the front shown in Fig. 5(b) is also encouraging. Data from the cooling source (CS) simulations of Mason *et al.* (2009) and Vermeire *et al.* (2011b), as well as additional liquid release experimental results, from Alahyari and Longmire (1995) are included in the figure. Alahyari and Longmire's (1995) experiments agree well with the other liquid release data but it is worth noting that both CS results show an increased width after impingement, compared to the experiments and URANS simulations, because the former were full-scale simulations that incorporated ground roughness, as opposed to the latter, which were laboratory-scale with a smooth surface.

4. Results and discussion

In this section, the temporal evolution of the downburst produced by the thunderstorm model is briefly discussed first and this is followed by spatial averaging of the wind field and, finally, the application of the scaling method to those downburst data.

4.1 Temporal evolution of the simulated thunderstorm downburst

From Orf *et al.* (2012) it is only possible to observe rather limited evidence of a "vortex-ring" like structure in the x-direction (East-West) because in the y-direction (both to the North and the South) the flow field is disturbed by adjacent smaller downburst events, typical of storm outflows which rarely comprise single, isolated events.

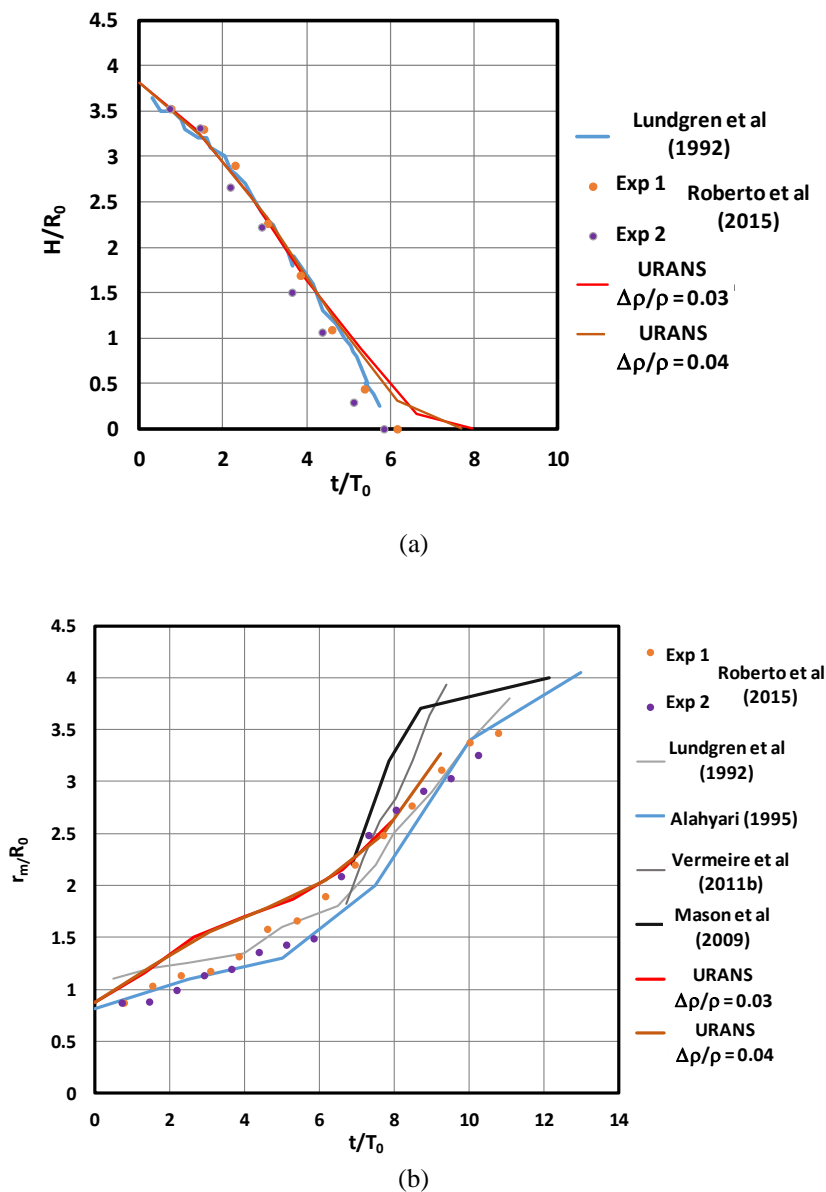
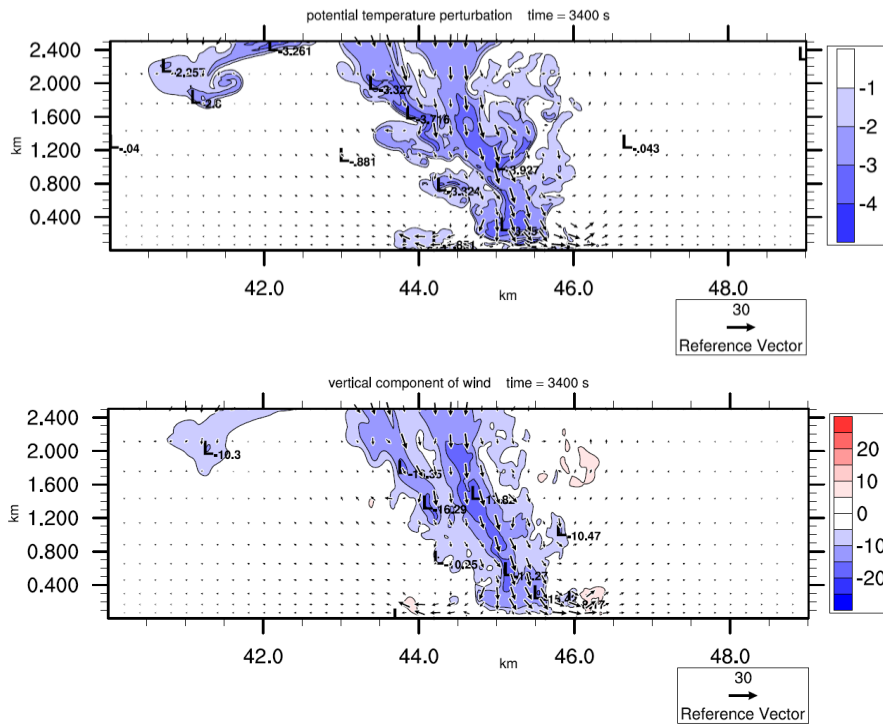


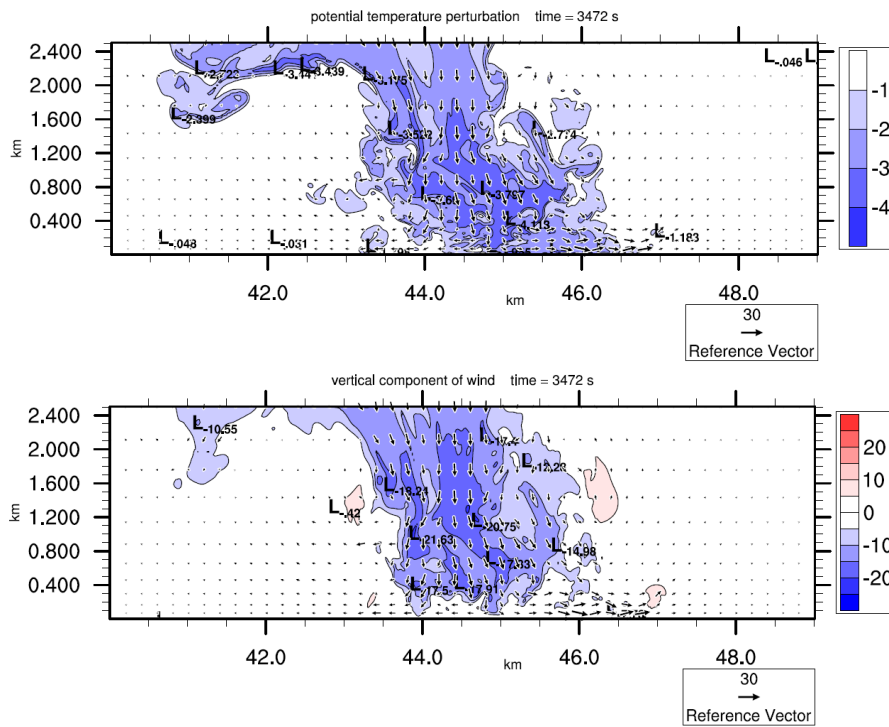
Fig. 5 Variation with time of (a) height (H) of downburst front above ground and (b) radius (r_m) of the downburst front

Fig. 6 shows vertical planes in this direction, through the centre of impingement, $(x,y) = (44.5 \text{ km}, 44.5 \text{ km})$, of the potential temperature perturbation followed by the vertical wind velocity component (with added vectors) for 6 time steps of $t = 3,400 \text{ s}, 3,472 \text{ s}, 3,588 \text{ s}, 3,606 \text{ s}, 3,628 \text{ s}$ and $3,744 \text{ s}$. At $t = 3,400 \text{ s}$, the area-averaged downdraft wind speeds (see Fig. 8, discussed in the next section) are starting to rapidly increase as are the radial wind speeds (see Fig. 9). From Fig. 6(a) it can be seen that the column of more dense air is tilted by about 22° from the vertical and, since it is these density gradients that force the downflow, the downdraft is also tilted by a similar angle in this plane. By $t = 3,472 \text{ s}$ the width of the strongly perturbed region and associated downdraft column has increased by about 50%, whilst the column has become more vertical. The

magnitudes of the radial wind speeds have reached about half of what will be their maximum values. The period encompassing $t = 3,588 \text{ s}, 3,606 \text{ s}$ and $3,628 \text{ s}$, represents the peak radial outflow regime of the downburst and is characterized by a large mass of the most dense air reaching the ground and spreading radially outwards within a layer extending up to about $z = 300 \text{ m}$. On the left hand (West) side of the event, this colder fluid is entrained into the vortex which has formed by $t = 3,588 \text{ s}$, but one cannot generalize about its structure as the vortex on the right hand (East) side is much more elongated in the horizontal direction. It is evident that, even as the peak radial wind speeds are occurring, there continue to be extensive density perturbations driving further downflows in this region, that persist until $t = 3,744 \text{ s}$ and beyond.

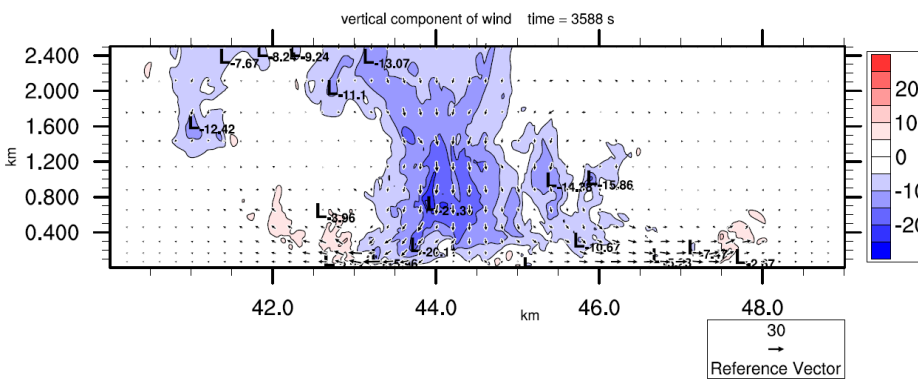
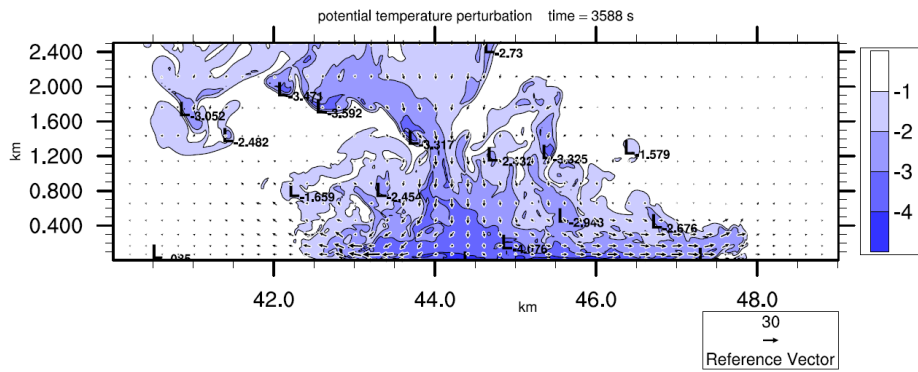


(a)

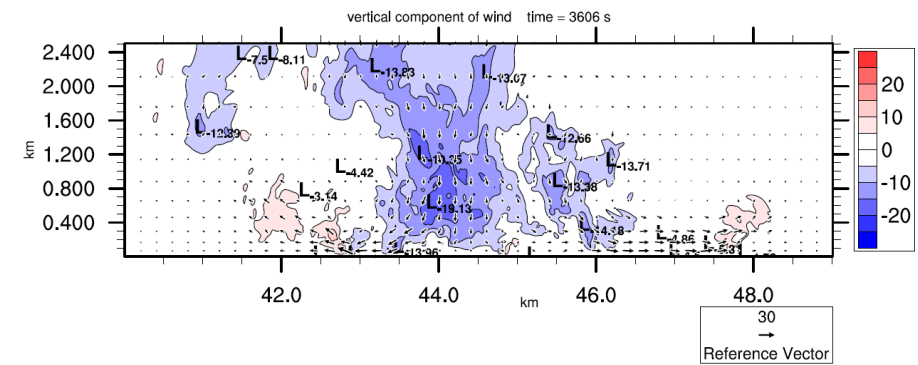
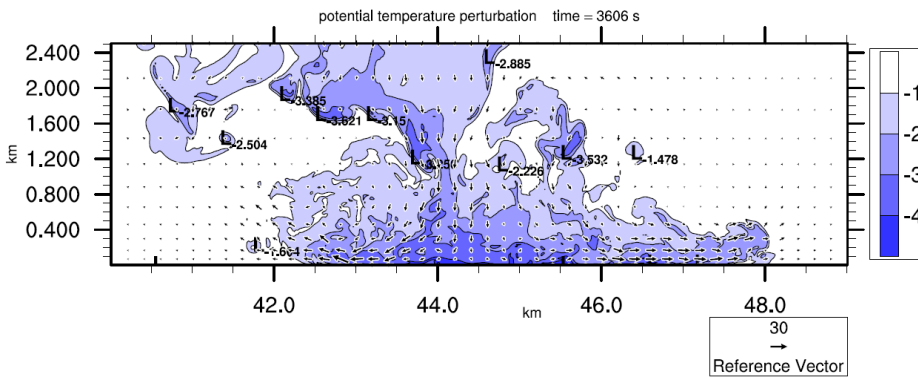


(b)

Continued-



(c)



(d)

Continued-

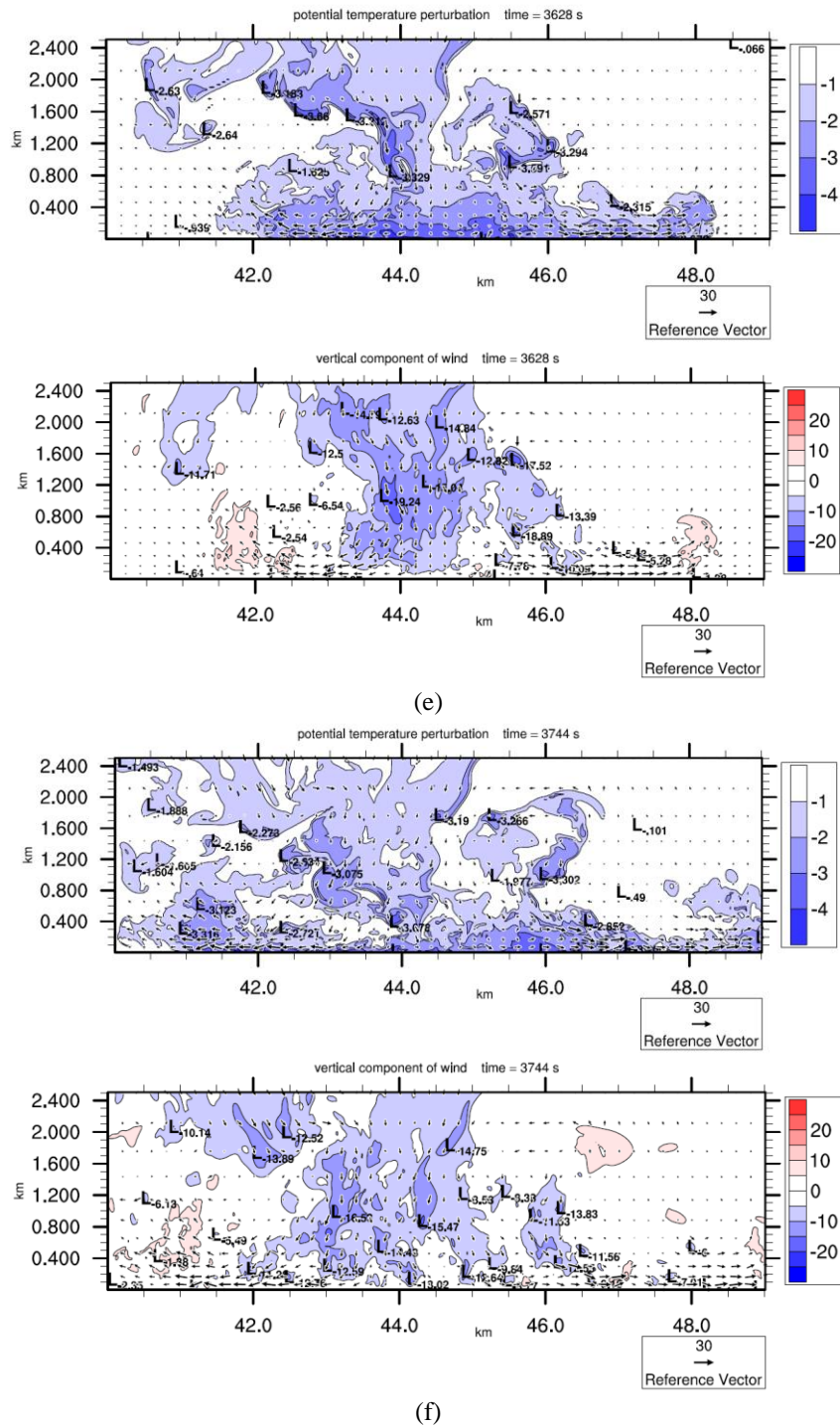


Fig. 6 Contours of potential temperature perturbation and vertical wind velocity component (with vectors) in vertical East-West (x-direction) plane through downburst centre at (a) $t = 3,400$ s, (b) $3,472$ s, (c) $3,588$ s, (d) $3,606$ s, (e) $3,626$ s and (f) $3,744$ s

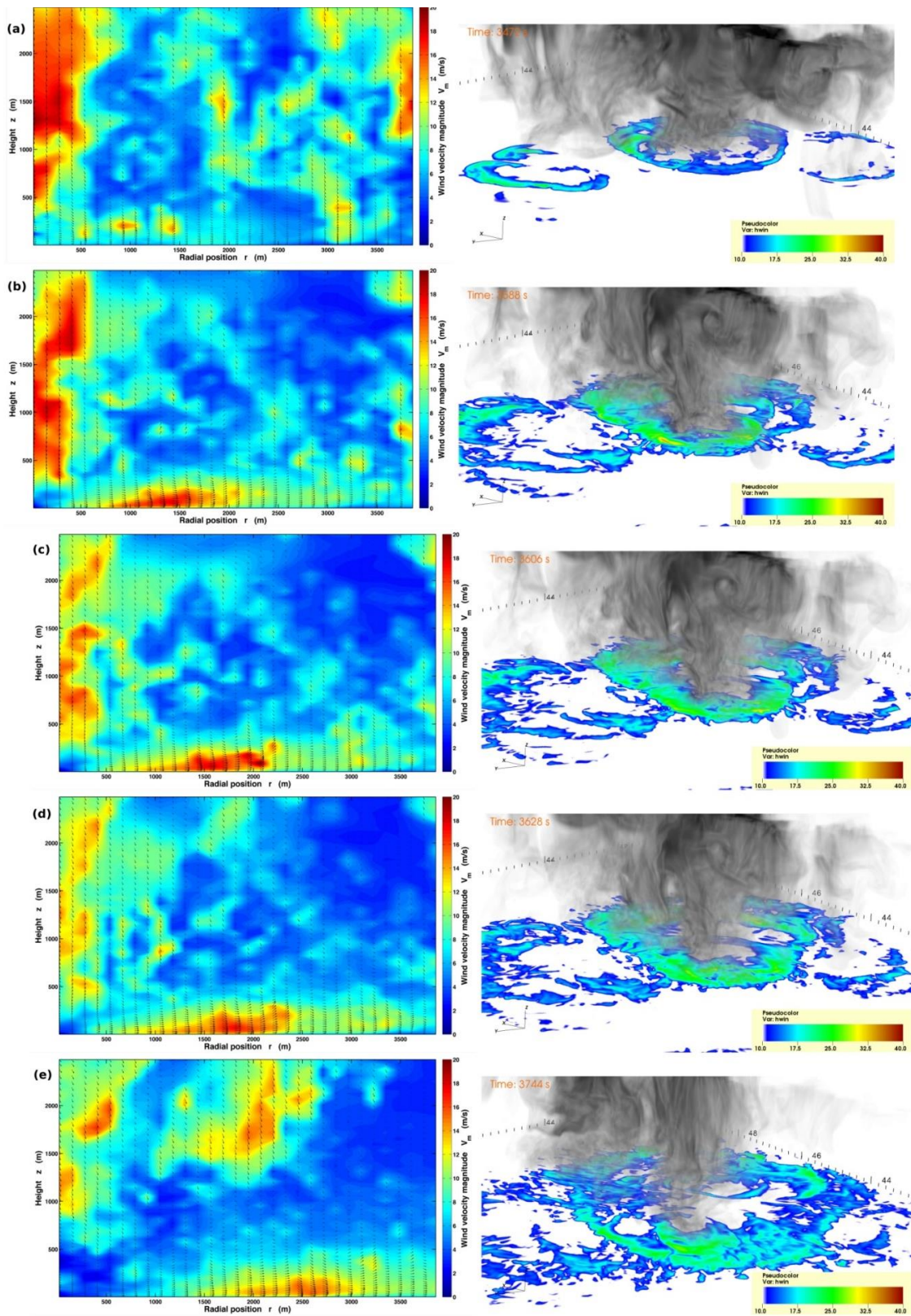


Fig. 7 Circumferentially-averaged velocity vectors in the vertical plane (r,z) and velocity magnitude contours, and snapshots of the sub-cloud region of the thunderstorm focused on the downburst. The grey volume in the frame is the rain mixing ratio, and the coloured horizontal (x,y) plane represents the horizontal wind speeds 19 m above ground level at: (a) $t = 3,472$ s, (b) $t = 3,588$ s, (c) $t = 3,606$ s, (d) $t = 3,628$ s and (e) $t = 3,744$ s

4.2 Spatial averaging of the simulated thunderstorm downburst

In order to provide a basis on which to compare the non axi-symmetric data of the thunderstorm simulation, to simpler axi-symmetric models, including the dense-fluid release model, it is necessary to process the raw data from the simulation. The full thunderstorm simulation produces an enormous amount of three-dimensional data, including wind velocity, potential temperature, pressure, and mixing ratios of water vapour, cloud water and ice, rain, snow, and graupel. The wind velocity vectors were simplified into an axi-symmetric form by spatial averaging around the circumference of the downburst descent column and radial outflow, for all the recorded time steps ($t = 3,002 \text{ s} - 3,998 \text{ s}$). In order to analyze the data in this way, the downburst origin was initially identified in horizontal cartesian coordinates (x, y) from the wind velocity vector field in the plane immediately above the ground. Then, at each radial distance (r) from the ground-impingement point, the radial (U_r) and vertical (U_z) components of the wind velocity vector were spatially averaged around the circumference of a circle of radius r . The vector field has been analyzed from the location of ground impingement ($r = 0 \text{ m}$) to the approximate maximum extent of the outflow ($r = 4,000 \text{ m}$), as well as in the vertical direction encompassing 120 individual heights. This method of analysis essentially simplifies the vector field to a two-dimensional domain (r, z) which consists of a base “axi-symmetric” flow, whilst facilitating comparison to existing studies.

Although the data suggest that peak wind speeds impinge upon the ground in an approximately circular pattern, their distribution is not axi-symmetric, illustrating the difference between full cloud simulations and more common studies involving CS, dense-fluid releases and IJ models. However, by reducing the vector field to a single (r, z) plane and plotting wind velocity contours of magnitude $V_m = (U_r^2 + U_z^2)^{1/2}$, a certain amount of the spatial variability and structure present prior to the circumferential averaging process is lost, whilst preserving the two regions of peak winds, as shown in Fig. 7.

This figure presents data from 5 time steps at $t = 3,472 \text{ s}$, $3,588 \text{ s}$, $3,606 \text{ s}$, $3,628 \text{ s}$ and $3,744 \text{ s}$ (coinciding with the temporal locations of Fig. 6 shown earlier). The visualizations of the flow field at each time step (rendered using rain mixing ratio and near-ground horizontal wind speed) in Fig. 7 show the non-uniformity of the downdraft column, when compared to any CS or IJ numerical or experimental simulation. It also shows that this column does not exist in isolation as there are two other events that form either side it.

Before considering how the complexity and spatial variability of this event might be modelled in a simpler manner, the key quantitative parameters arising from analysis (Orf *et al.* 2012, 2014) of this simulated thunderstorm downburst will be summarized here. Note that all these metrics are, by the nature of the event, very approximate and indicative of “average” values for this single simulated thunderstorm alone. As noted earlier, the main downburst event is approximately centred at (x, y) =

(44.5 km, 44.5 km) within the computational domain. From the circumferentially-averaged wind speed fields (such as those shown in Fig. 7) the diameter of downdraft column of this main event is roughly 1,300 m. The temperature perturbation, giving rise to an approximately equivalent density perturbation, is about 4 K in 300 K, which is a 1.33% difference from the ambient. Although it is extremely difficult to define a discrete “source” location for the downburst fluid the cloud base is at about 3,300 m AGL and the “source” is associated with the rain field beneath this and so one might estimate the “source” height to be of the order of 2,500 m or roughly twice the diameter of the downburst column. The descending column of air commences at about 3,000 s into the simulation with the peak downdraft wind speeds occurring at about 3,500 s and the peak radial outflow at around 3,600 s (the best estimate for the difference in these peak times is 120s). The localized maximum downwards wind speed in the downdraft column is about 23 m/s with this peak downdraft value found at a height ranging from 1.5 km to 0.8 km, over the time range from 3,512 s – 3,564 s. However, as indicated from Figs. 7(a) and 7(b) a better estimate, covering a larger region of the centre of the downdraft column, would be a maximum of around 18 m/s.

From the circumferentially-averaged data the maximum radial wind speeds occur at a radial distance of $r = 1,500 \text{ m}$ from impingement, with the highest circumferentially-averaged radial wind speed being about 17.5 m/s and the corresponding peak value being about 35 m/s. In general, it is found that the peak radial wind speed around any circumference is approximately twice the averaged value. The height to the peak at $r = 1,500 \text{ m}$ is about $z = 50 \text{ m}$. It was noted earlier that the characteristic “ring vortex” was only evident, to some extent, in the East-West (x -direction). Where it is visible in the velocity field it has a linear scale of the order of 1,500 m.

Considering the vertical wind speed component in the downdraft column, Fig. 8 shows, at each height, the time history contours of the *area-averaged* vertical wind speed (averaged over the horizontal cross-section of the downdraft column of diameter 1,300 m). This gives a much lower maximum downwards speed of approximately 16 m/s (compared to the 18 m/s mentioned earlier that represents the highest values near the centre of the column). In contrast to any simple axi-symmetric downburst model, the variation of maximum vertical wind speeds with time in the downdraft column shown here appears to depict a series of vertical profiles that are angled from the left to the right when descending towards the ground, resulting in bands of wind speed peaks. Since the peak radial wind speed occurs at about 3,600 s, only some of these high vertical wind speed regions subsequently contribute to that peak (those occurring nearer the ground at around 3,500 s). It may be seen that there is a general downdraft flow (negative vertical velocities) over all heights and at all times (persisting for at least the 17 mins shown in the figure), except for the relatively weak upflow below 1,500 m height from 3,300 – 3,400 s which is accompanied by a strengthening of the downwards winds at heights above this.

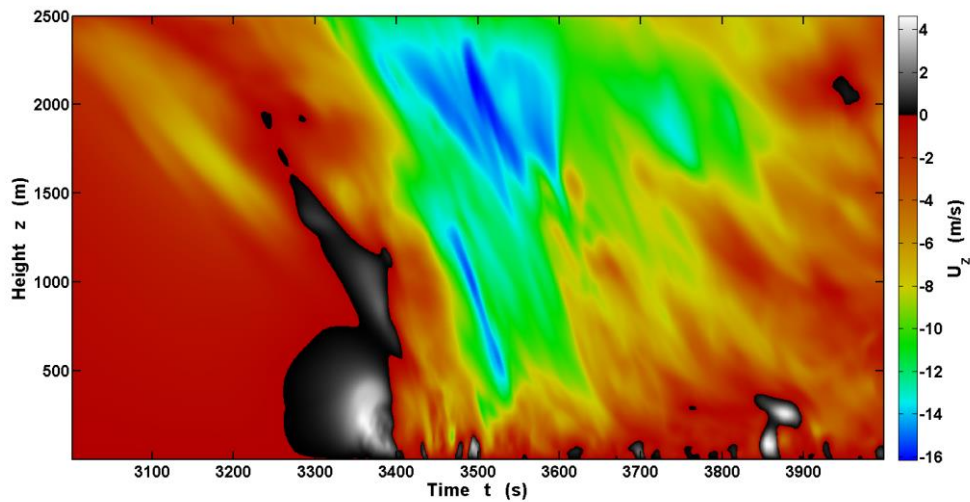


Fig. 8 Variation of vertical wind speed with time within the downdraft vertical “cylindrical” column, spatially averaged over that column cross-sectional area (of diameter = 1,300 m)

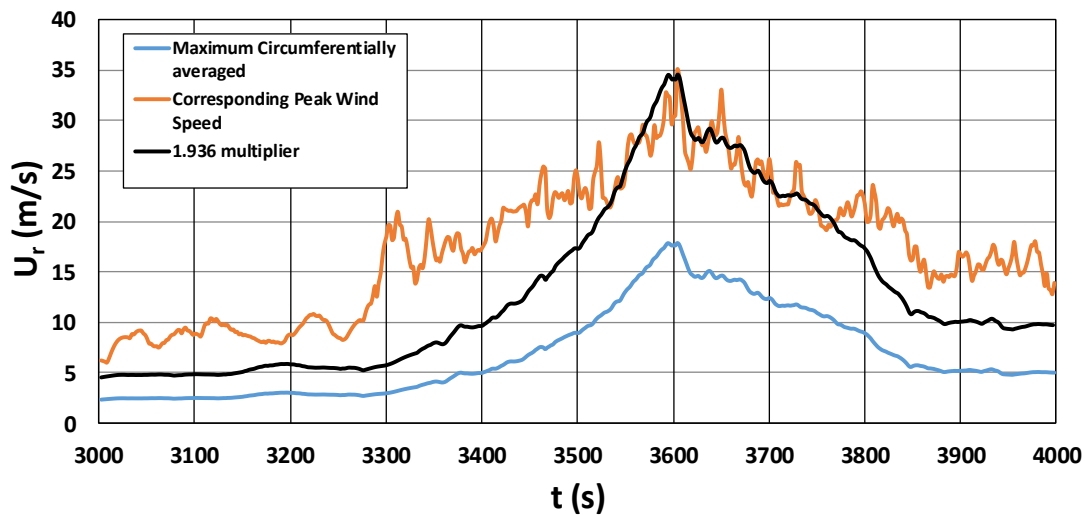


Fig. 9 Variation with time of the maximum circumferentially-averaged radial wind speed at the radial location corresponding to its maximum value ($r = 1,500$ m), together with the peak value around the circumference at each time

In the case of an axi-symmetric downburst simulated in a non-moving framework (no wind shear or environmental winds), with the centre of the reference downburst circle centred on the centre of the downdraft, one would expect the corresponding plot to look very plain in comparison. For example, it would show a single downdraft descending (with a similar slope), a part of the ring vortex and then very little else as the outflow moves beyond the 650 m radius of the column. The fact that the present simulation shows so much structure is a consequence of not only the asymmetry and the fact that multiple events are occurring, but also because the reference circle centre does not remain in the “true” centre of the downdraft during its entire and extensive lifetime.

Related to these vertical wind speed time history data, Fig. 9 shows the variation with time of the maximum value of the circumferentially-averaged radial outflow velocity at the location where the peak radial wind speed occurs ($r = 1,500$ m). It will be seen that there is an environmental wind speed of about 2 m/s prior to the downburst outflow that is due to the earlier downdrafts in this region. It was previously found (Orf *et al.* 2014) that for times at and near to the occurrence of the peak radial outflow wind speed the peak radial wind speed could be approximated by the circumferentially-averaged value multiplied by 1.936. Fig. 9 also shows the variation of the peak value around the circumference at $r = 1,500$ m, together with the mean value multiplied by 1.936. This shows that, whilst this multiplier

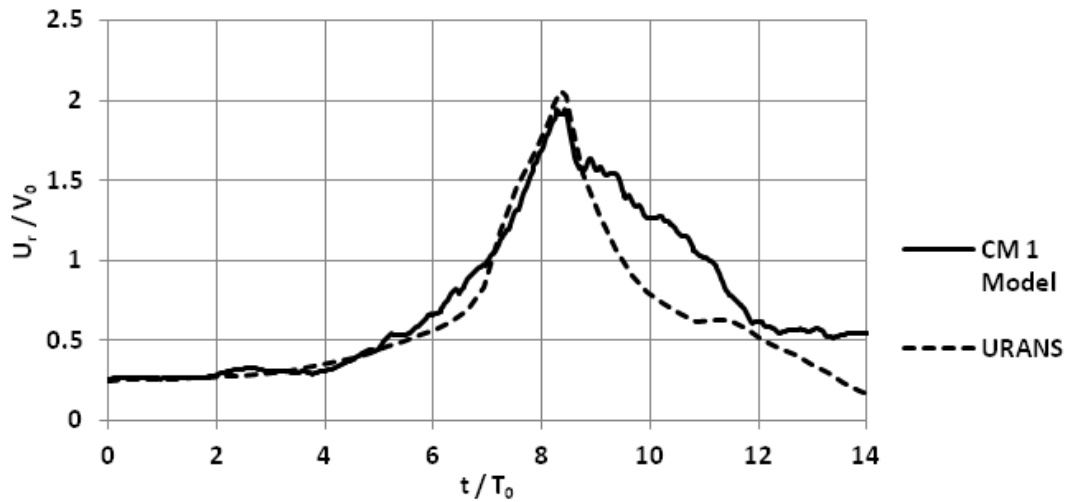


Fig. 10 Scaling of the time history of the circumferentially-averaged peak radial wind speed at location of maximum radial wind speed for both the URANS model and CM1 thunderstorm model data

consistently under-estimates the peak wind speeds both prior to the maximum value (which occurs at about 3,600 s) and during the tail of the event, it works extremely well for the period 1 min before the maximum to 3 min afterwards. Indeed, one would not expect to see a strong correlation between the spatially-averaged mean and peak wind speed near the ground at times prior to 3,500 s since, although the main downburst is reaching the ground around that time, the near-ground wind speeds are more characteristic of the several other, smaller, events that have occurred previously in that region.

4.3 Scaling of the thunderstorm model downburst

The results from the URANS simulations, described in section 2.2, for liquid releases from a cylinder with $R_0 = 4.31$ cm whose base is located at $H_0 = 3.81 R_0$ above the ground, show that the maximum radial velocity is $U_{r,\max} = 1.81 V_0$. The radial location at which this occurs is $r_{\max} = 2.41 R_0$ and the height to the maximum radial velocity is $z_{\max} = 0.23 R_0$.

In the absence of a well-defined “source” for the downburst fluid in the thunderstorm simulation, the best estimate for the radial length scale is half of the downburst column diameter, namely $R_0 \approx 650$ m, which, for a “source” base height of 2,500 m, gives $H_0 \approx 3.85 R_0$, which is very similar to the URANS model source location of $3.81 R_0$. Using the estimate of $\Delta\rho/\rho = 0.0133$ from the thunderstorm simulation, together with Eq. 1, the other scaling parameters become $T_0 \approx 70.5$ s and $V_0 \approx 9.2$ m/s. Based on the URANS results, it is found that the predicted full-scale values are; $U_{r,\max} = 16.6$ m/s (a 5% difference compared to the circumferentially-averaged simulated value of 17.5 m/s), $r_{\max} = 1,566$ m (a 4% difference from the simulation estimate of 1500 m) and $z_{\max} = 150$ m (a 200% difference from the simulation estimate of 50 m). The discrepancy in z_{\max} is most probably attributed to the difference in ground roughness between the two cases, although, as shown in Orf

et al. (2014), at this radial location z_{\max} varies over a range of 38 – 70 m within only 20 s of the peak velocity time). In addition, the time from the initiation of the downdraft to when the maximum radial wind speed occurs was found from the URANS simulations to be $t_{\max} = 8.37 T_0$, which gives $t_{\max} = 590$ s (a 2% difference compared to the very approximate CM1 simulation estimate of 600 s). Furthermore, the maximum downwards wind speed in the downdraft column was found from the URANS simulations to be $U_{z,\max} = 2.24 V_0$ (note that Lundgren *et al.* (1992) have a similar value of $U_{z,\max} = 2 V_0$) which gives $U_{z,\max} = 20.6$ m/s (a 14% difference from the estimated CM1 simulation maximum value of 18.0 m/s).

Fig. 10 compares the time history of the circumferentially-averaged maximum radial wind speed, at the radial location of its maximum value (shown earlier in Fig. 9), with the results from the present URANS model, both scaled using the parameters from Lundgren *et al.* (1992). An offset of $\Delta U_r/V_0 = 0.25$ has been added to the URANS data to account for the environmental wind speed present in the downburst produced by the thunderstorm simulation, noted earlier. It may be seen that the agreement is extremely close up to and immediately following the peak and within 30% after that. At this stage, one can only say that the results of these comparisons are encouraging, especially given the significant difference in the Re of the two simulations (being around $Re = 5 \times 10^3$ in the URANS and $Re = 4.0 \times 10^8$ in the present work) and, hence, in geometrical scale (which is approximately 1:15,000), together with the vastly more complex and detailed flow structure within the simulated thunderstorm outflow. The similarity in these outflow time histories does, therefore, indicate that the large-scale dynamics are inviscid, with both the simple URANS model of liquid releases and the thunderstorm downburst outflow demonstrating, to the first order, a conversion of potential energy to kinetic energy and, hence, a non-linear relationship between “source strength” and the outflow wind speeds.

5. Conclusions

Downburst events are always far from axi-symmetric in nature and may be preceded and/or followed by other downdrafts from the parent storm. Hence, it is a challenge to represent such real events by using simple axi-symmetric modelling approaches applied to a single downburst in isolation within a quiescent environment. Here, a complete downburst-producing thunderstorm has been simulated using a full-scale cloud model (CM1), which is a Large Eddy Simulation model, incorporating a sub-grid turbulence model and micro-physics parameterizations. The main downburst event arising from this simulation has a downdraft column diameter of about 1,300 m and peak radial outflow wind speeds of around 38 m/s. Thus, it represents a moderate, rather than extreme, event in terms of size and intensity. For comparison purposes, a very simple, reduced-scale, simple axi-symmetric, density-driven downburst model was also implemented, in Unsteady Reynolds-Averaged Navier-Stokes (URANS) simulations with the $k-\omega$ turbulence closure incorporating the low-Reynolds number correction. The present work has shown that the non-linear relationship between “source” strength, as represented by a potential temperature (or density) perturbation, and the strength of the near-ground radial outflow appears to replicate the results from a downburst-producing thunderstorm simulation very well when compared to a simpler axi-symmetric, constant density, dense-source model. This is in contrast to the impinging jet model, commonly used in wind engineering, where the relationship between a specified “jet” velocity (which is clearly not a specified “source” strength) and the resulting radial outflow wind speeds is linear. It has also been shown that the evolution of the vertical winds within the downburst column is significantly more complex than that occurring in any simpler (CS, dense-fluid release or IJ) model. There is a long period of mostly downwards winds (persisting for at least 17 mins in the present simulation), at heights up to at least 2,500 m, within which bands of strengthening then weakening higher magnitude downwards wind speeds occur only some of which contribute to the peak radial outflow winds within the main downburst event.

Acknowledgments

The work is supported by the Natural Sciences and Engineering Research Council (NSERC) of Canada, the Ontario Graduate Scholarship (OGS) program, the National Center for Super-computing Applications (NCSA) and the National Center for Atmospheric Research (NCAR). The authors are grateful to G. Bryan for use of his CM1 cloud model. The simulations were conducted on NCSA’s IBM POWER575+ Blueprint cluster, which was made accessible via National Science Foundation (NSF) Grant 09-41392.

References

Abd-Elaal, E.S., Mills, J.E. and Ma, X. (2013), “A coupled

- parametric-CFD study for determining ages of downbursts through investigation of different field parameters”, *J. Wind Eng. Ind. Aerod.*, **123**, 30-42.
- Aboshosha, H. and El Damatty, A. (2015), “Engineering method for estimating the reactions of transmission line conductors under downburst winds”, *Eng. Struct.*, **99**, 272-284.
- Alahyari, A. (1995), “Dynamics of laboratory simulated microbursts”, Ph.D. Thesis, Univ. Minnesota, U.S.A.
- Alahyari, A. and Longmire, E.K. (1994), “Particle image velocimetry in a variable density flow: application to a dynamically evolving downburst”, *Exp. Fluids*, **17**, 434-440.
- Alahyari, A. and Longmire, E.K. (1995), “Dynamics of experimentally simulated microbursts”, *AIAA J.*, **33**, 2128-2136.
- Anabor, V., Rizza, U., Nascimento, E.L. and Degrazia G.A. (2011), “Large-Eddy Simulation of a microburst”, *Atmos. Chem. Phys.*, **11**, 9323-9331.
- Anderson, J.R., Orf, L.G. and Straka, J.M. (1992), “A 3-D model system for simulating thunderstorm microburst outflows”, *Meteorol. Atmos. Phys.*, **49**, 125-131.
- Brown, J.M., Knupp, K.R. and Caracena, F. (1982), “Destructive winds from shallow high-based cumulonimbi”, *Preprints of 12th Conf. Severe Local Storms.*, Am. Meteor. Soc., Boston, U.S.A., 272-275.
- Bryan, G.H. and Fritsch, J.M. (2002), “A benchmark simulation for moist non-hydrostatic numerical models”, *Mon. Weather Rev.*, **130**, 2917-2928.
- Burlando, M., Romanic, D., Solari, G., Hangan, H. and Zhang, S. (2017) “Field data analysis and weather scenario of a downburst event in Livorno, Italy on 1 October 2012”, *Mon. Weather Rev.*, **145**, 3507-3527.
- Gunter, W.S. and Schroeder, J.L. (2015) “High-resolution full-scale measurements of thunderstorm outflow winds”, *J. Wind Eng. Ind. Aerod.*, **138**, 13-26.
- Holmes, J.D., Hangan, H.M., Schroeder, J.L., Letchford, C.W. and Orwig, K.D. (2008), “A forensic study of the Lubbock-Reese downdraft of 2002”, *Wind Struct.*, **11**, 19-39.
- Kim, J. and Hangan, H. (2007), “Numerical simulations of impinging jets with application to thunderstorm downbursts”, *J. Wind Eng. Ind. Aerod.*, **95**, 279-298.
- Letchford, C.W. and Chay, M.T. (2002), “Pressure distributions on a cube in a simulated thunderstorm downburst. Part B: Moving downburst observations”, *J. Wind Eng. Ind. Aerod.*, **90**, 733-753.
- Lombardo, F.T., Smith, D.A., Schroeder, J.L. and Mehta, K.C. (2014), “Thunderstorm characteristics of importance to wind engineering”, *J. Wind Eng. Ind. Aerod.*, **125**, 121-132.
- Lundgren, T.S., Yao, J. and Mansour, N.N. (1992), “Microburst modelling and scaling”, *J. Fluid Mech.*, **239**, 461-488.
- Mason, M.S., Wood, G.S. and Fletcher, D.F. (2009), “Numerical simulation of downburst winds”, *J. Wind Eng. Ind. Aerod.*, **97**, 523-539.
- Orf, L. and Anderson, J. (1999), “A numerical study of traveling microbursts”, *Mon. Weather Rev.*, **127**, 1244-1258.
- Orf, L.G., Kantor, E. and Savory, E. (2012), “Simulation of a downburst-producing thunderstorm using a very high-resolution three-dimensional cloud model”, *J. Wind Eng. Ind. Aerod.*, **104-106**, 547-557.
- Orf, L.G., Oreskovic, C., Savory, E. and Kantor, E. (2014), “Circumferential analysis of a simulated three-dimensional downburst-producing thunderstorm outflow”, *J. Wind Eng. Ind. Aerod.*, **135**, 182-90.
- Roberto, M., Savory, E. and Porto, J. (2015), “Experimental and numerical simulation of density-driven thunderstorm downbursts”, *Proceedings of the 14th Int. Conf. Wind Eng.*, Porto Alegre, Brazil, June.
- Sengupta, A., Sarkar, P.P. and Rajagopalan, G. (2001), “Numerical and physical simulation of thunderstorm downdraft

- winds and their effects on buildings”, *Proceedings of the 1st Amer. Conf. Wind Eng.*, Clemson, U.S.A., June.
- Sengupta, A. and Sarkar, P.P. (2008), “Experimental measurement and numerical simulation of an impinging jet with application to thunderstorm microburst winds”, *J. Wind Eng. Ind. Aerod.*, **96**, 345-365.
- Shehata, A.Y., El Damatty, A.A. and Savory, E. (2005), “Finite element modeling of transmission line under downburst wind loading”, *J. Finite Elem. Anal. Des.*, **42**, 71-89.
- Solari, G., Burlando, M., De Gaetano, P. and Repetto, M.P. (2015), “Characteristics of thunderstorms relevant to the wind loading of structures”, *Wind Struct.*, **20**, 763-791.
- Vermeire, B.C., Orf, L.G. and Savory, E. (2011a), “A parametric study of downburst line near-surface outflows”, *J. Wind Eng. Ind. Aerod.*, **99**, 226-238.
- Vermeire, B.C., Orf, L.G. and Savory, E. (2011b), “Improved modelling of downburst outflows for wind engineering applications using a cooling source approach”, *J. Wind Eng. Ind. Aerod.*, **99**, 801-814.
- Yao, J. and Lundgren, T.S. (1996), “Experimental investigation of microbursts”, *Exp. Fluids*, **21**, 17-25.
- Zhang, Y., Hu, H. and Sarkar, P.P. (2013), “Modeling of microburst outflows using impinging jet and cooling source approaches and their comparison”, *Eng. Struct.*, **56**, 779-793.
- Zhang, S., Solari, G., De Gaetano, P., Burlando, M. and Repetto, M.P. (2017), “A refined analysis of thunderstorm outflow characteristics relevant to the wind loading of structures”, *Probabilist. Eng. Mech.*, DOI: 10.1016/j.probengmech.2017.06.003.

